Supplementary Materials:

Janus Monolayer Transition Metal Dichalcogenides

Jing Zhang[1‡], Shuai Jia[1‡], Kholmanov Iskandar[2], Liang Dong[3], Dequan Er[3], Weibing Chen[1], Hua Guo[1,] Zehua Jin[1], Vivek B. Shenoy[3], Li Shi[2] and Jun Lou[1*]

Descriptor of the HER Efficiency: The catalytic efficiency of TMDs for HER is characterized by hydrogen adsorption free energy ΔG_H[1]. A positive ΔG_H indicates weak absorption of hydrogen atoms on the surfaces of TMDs in the initial stage of HER, which reduces the probability of subsequent reactions. On the contrary, a negative ΔG_H indicates strong binding of H atoms on the surfaces, which prevents the detachment of H_2 molecules from the catalyst. The optimal value of ΔG_H is 0 eV, i.e., thermally neutral. ΔG_H is defined as

$$\Delta G_H \ = \ \Delta E_H + \Delta E_{ZPE} - T\Delta S. \tag{1}$$

In the above equation, ΔE_H is the differential hydrogen adsorption energy, and is calculated by

$$\Delta E_H \ = \ E(SMoSe + H) - E(SMoSe) - \frac{1}{2}E(H_2), \tag{2}$$

where $E(SMoSe + H)$, $E(SMoSe)$, and $E(H_2)$ represent the total energy of SMoSe with one H atom absorbed on the surface, the energy of SMoSe with clean surface, and the energy of a H_2 molecule, respectively. ΔE_{ZPE} in Eq. (1) is the difference in zero-point energy between the adsorbed hydrogen and hydrogen in the gas phase, and is calculated from the vibrational frequencies of the H atom at 0K. Finally, T and ΔS in Eq. (1) are the temperature (set to be 300K) and the entropy difference between absorbed H and H in the gas phase, respectively. In our calculations, the configurational entropy of the H atom in the adsorbed state is small and is neglected. Therefore, $\Delta S = -1/2\ S(H_2)$ where $S(H_2)$=130.68 J·mol^{-1}·K^{-1} is the entropy of the H_2 molecule in the gas phase at standard conditions: 1 bar of H_2, pH = 0 and T = 300 K[2].

HER Device Fabrication and Measurement: The SMoSe monolayer on SiO_2 was etched off and transferred onto another SiO_2 substrate by the PMMA-assisted wet transfer method[3]. The SiO_2 substrate has markers and electrode pads fabricated in advance of the transfer process. The electrode pads were then connected to the SMoSe by ebeam lithography and ebeam evaporation of Ti/Au. Another layer of PMMA was spin-coated onto the device afterwards and patterned with ebeam lithography method to expose exclusively the basal plane region of the monolayers (Figure S9). 0.5M H_2SO_4 bubbled with ultra-high purity nitrogen for 10 min was used as the electrolyte. A droplet of H_2SO_4 was dropped onto the sample region while a carbon wire and a Ag/AgCl wire were dipped into the H_2SO_4 droplet and used as the counter and reference electrode for the electrochemical measurements. CHI 650D electrochemical station was used to collect all the HER data.

SeMoS sample was fabricated following this procedure: The etched-off PMMA film with SMoSe monolayers attached was scooped up with a wafer, and slowly moved onto a Petri

dish filled with DI water. Due to the surface tension of the water, the PMMA film spontaneously detaches from the wafer and flow onto the water surface. The PMMA film was then scooped up with the device substrate and dried naturally, leaving a SeMoS/PMMA/SiO$_2$ construction. Acetone was added to the PMMA in a dropwise fashion, etching the PMMA as well as preventing the SeMoS from drifting. After completely dissolving the PMMA, the SeMoS device was successfully fabricated (Figure S11), ready for the following procedure.
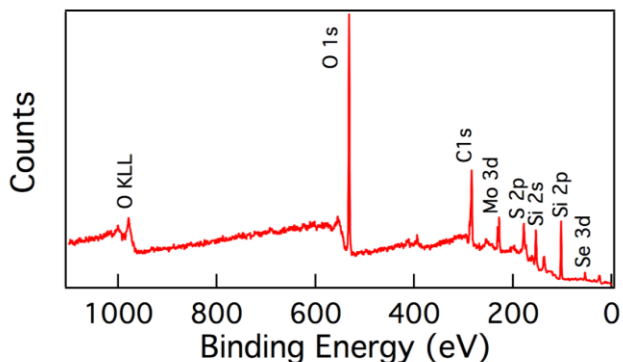

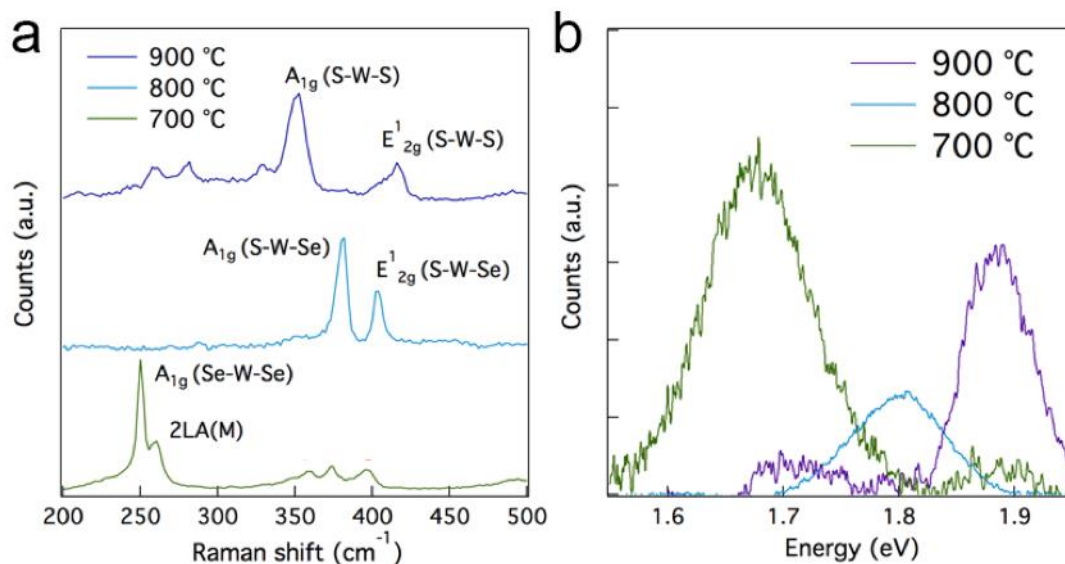Figure S1. Survey scan of the Janus SMoSe monolayer on SiO$_2$/Si wafer.

Figure S2. (a) Raman and (b) PL spectra of WSe$_2$ after being sulfurized at different temperatures. At 700 ^{o}C (green) the Raman spectra remains similar to pristine WSe$_2$, with emerging peaks originated from the scattered surface selenium substitution located between 350 to 400 cm^{-1}. At 800 ^{o}C (blue) two characteristic peaks are observed, indicating the formation of the Janus SWSe structure. At 900 ^{o}C (purple) the spectra

evolve into the WS$_2$ analogue, implying the complete selenium substitution by sulfur. The PL spectra show the similar evolution trend with MoSe$_2$.
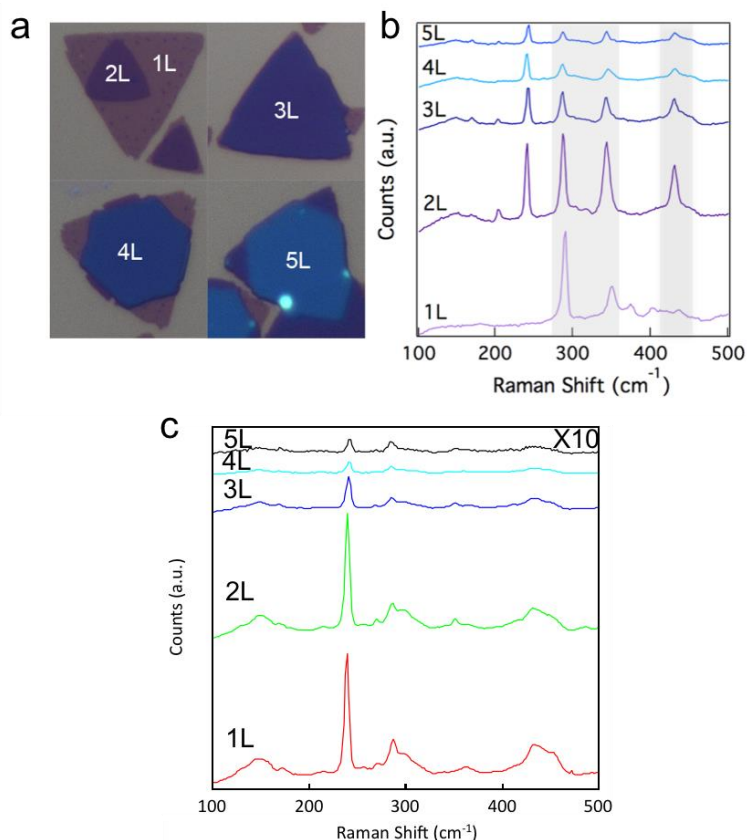

Figure S3. Raman evolution of SMoSe and MoSe$_2$ from monolayer to multilayers. (a) MoSe$_2$ flakes with increasing number of layers. The contract of the MoSe$_2$ develops from light purple to light blue as the number of layer increases. (b) Layer number dependence on the Raman of Janus SMoSe on MoSe$_2$ flakes. The gray background region highlights the evaluation of the Raman characteristic peaks of the Janus SMoSe. (c) Raman spectra of MoSe$_2$ with various layer numbers as comparison. Besides the A$_{1g}$ and E$^1_{2g}$ peaks, the peaks around 150 cm^{-1}, 350 cm^{-1} (visible when layer number exceeds two), 430 cm^{-1} and 450 cm^{-1}, have all been reported as the MoSe$_2$ Raman signals[4, 5, 6].
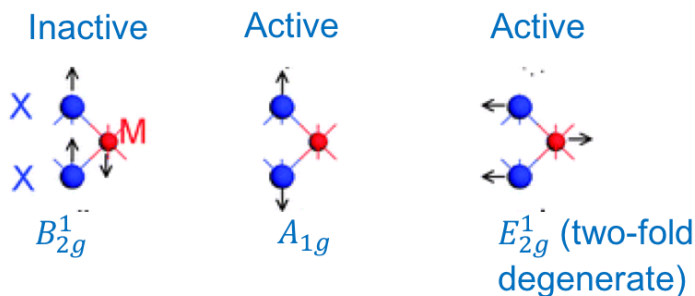
Figure S4. Schematic illustration of the lattice vibration modes in MX_2 metal dichalcogenides. The B^1_{2g} mode is only active while the top and bottom atoms are not identical.
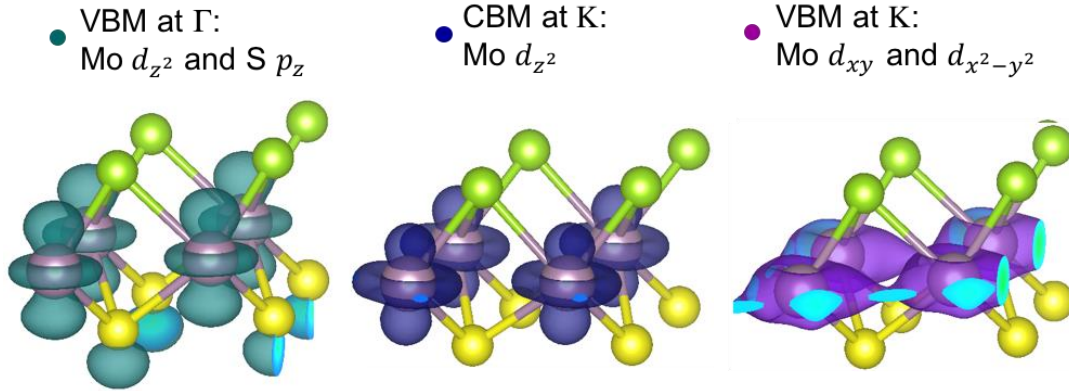
● VBM at Γ:
Mo d_{z^2} and S p_z

● CBM at K:
Mo d_{z^2}

● VBM at K:
Mo d_{xy} and $d_{x^2-y^2}$

Figure S5. Charge density distribution of VBM at Γ point (green), CBM at K point (blue) and VBM at K point (purple) of monolayer Janus SMoSe.
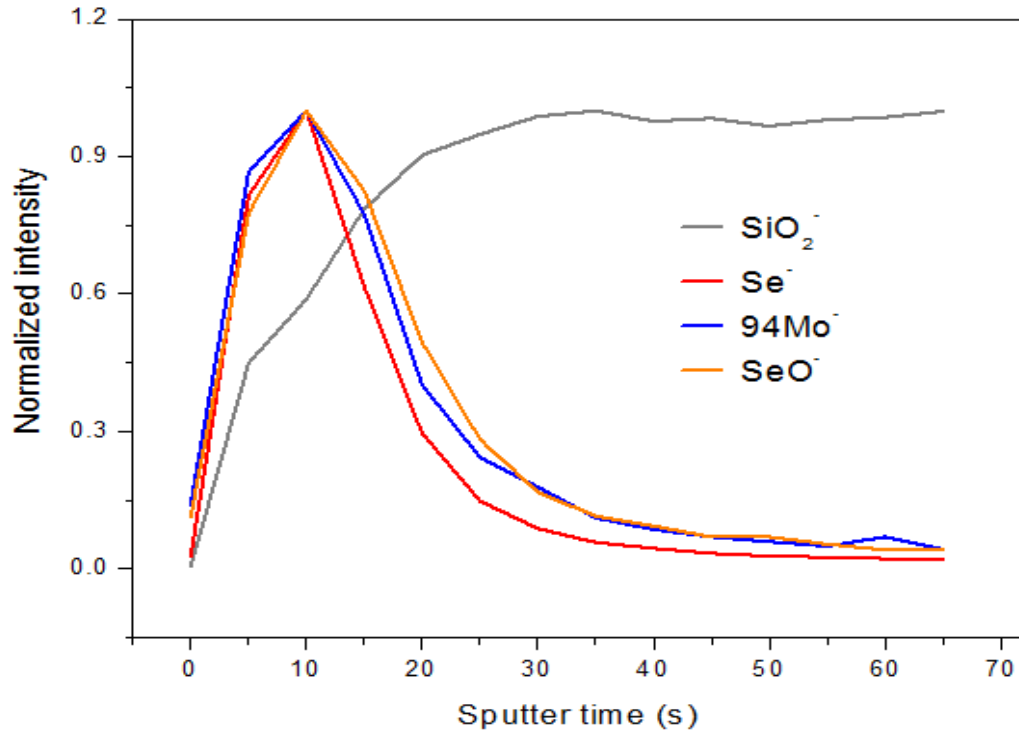

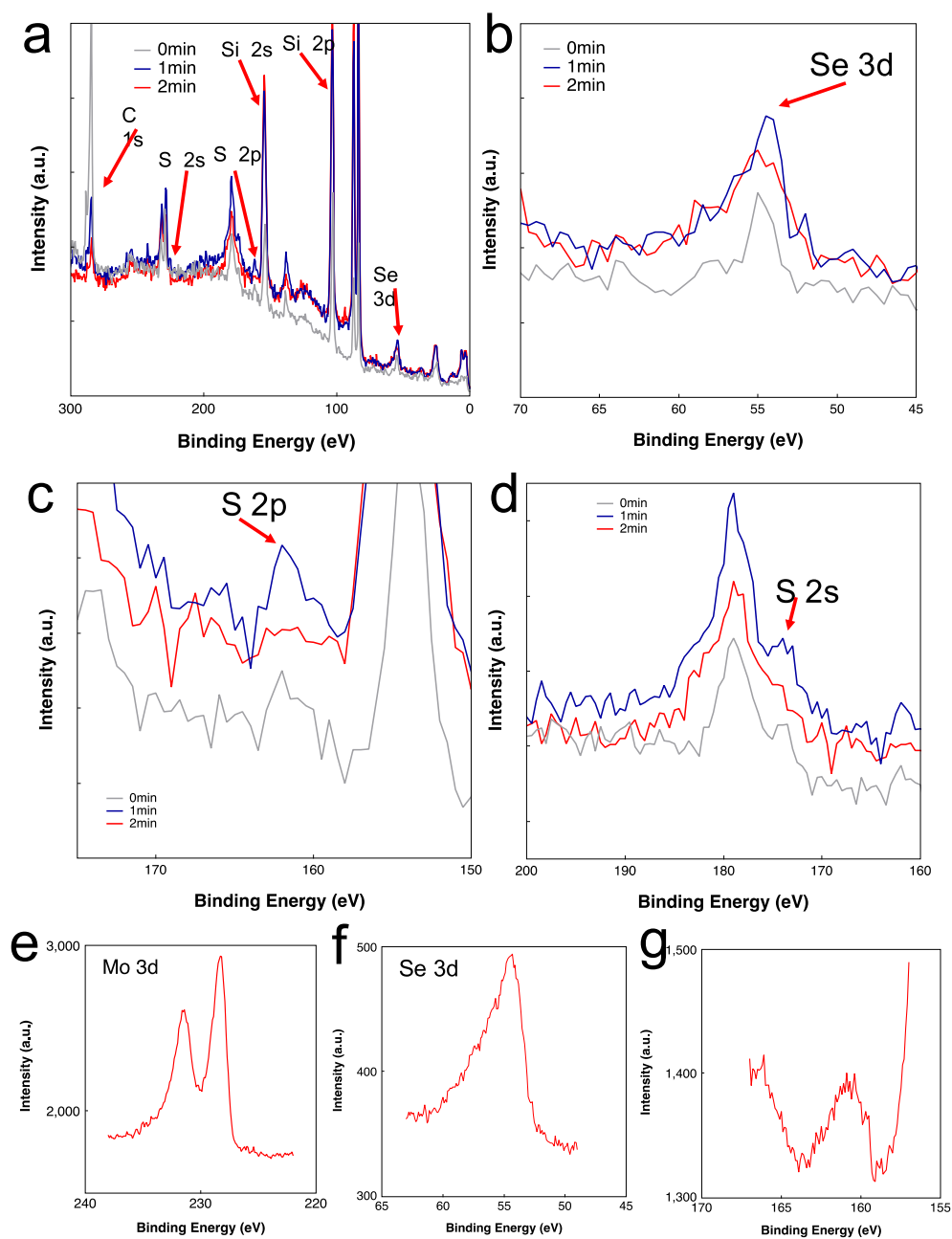Figure S6. TOF-SIMS of pure $MoSe_2$.

Figure S7. XPS profile analysis on the Janus SMoSe monolayer. (a) Survey spectra of samples with 0 to 2 min sputtering. C 1s, Si 2s and 2p, S 2s and 2p, Se 3d signals are indicated. (b)-(d) Detailed spectra on Se 3d, S 2p, Mo 3d and S 2s peaks. (e)-(g) Accumulated spectra on Mo 3d, Se 3d and potential S 2p region after 2 min sputtering.
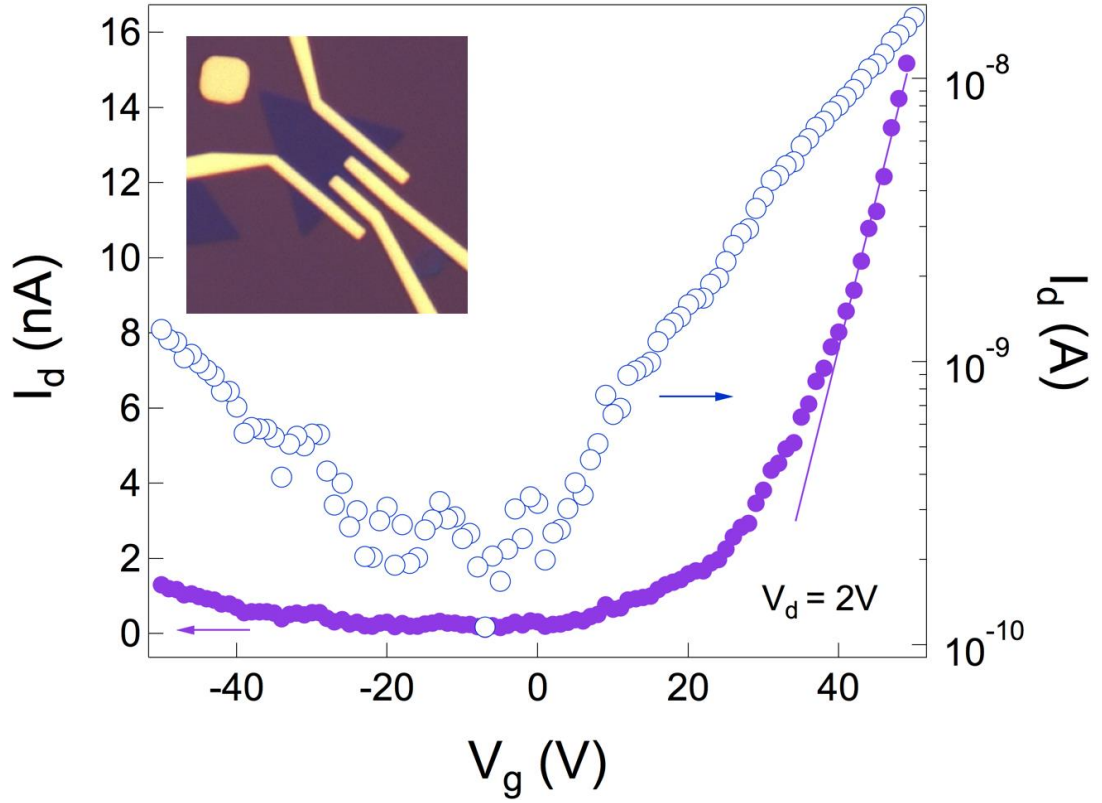
Figure S8. (Solid circles) Drain-source current I_d as a function of back-gate voltage V_g at fixed drain-source bias voltage $V_d = 2$ V. (Solid line) Linear fit of the data within the back gate voltage range from $40 - 50$ V. The carrier mobility based on the linear fit data is calculated to be m $= 0.06$ cm^2 V^{-1} s^{-1}. (Hollow circles) Corresponding I_d plotted in logarithmic scale as a function of back-gate voltage V_g at fixed drain-source bias voltage $V_d = 2$ V. Inset shows the optical image of a typical Janus SMoSe field-effect transistor device.
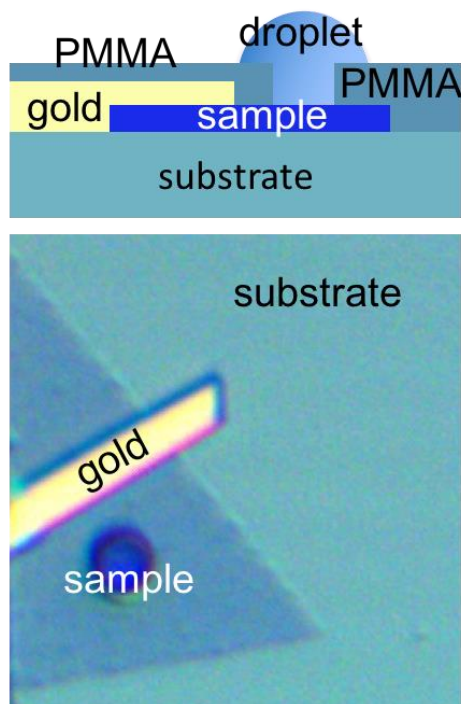
Figure S9. HER measurement device. On top is the schematic illustration of the device. The edge of the sample is completely covered by the PMMA layer and only the basal plane of the sample is exposed to the electrolyte, enabling the basal-plane-exclusive measurements of the Janus samples. At bottom is the optical image of the device. A circular HER window is fabricated by ebeam lithography locating on the basal plane region of the triangular flake.
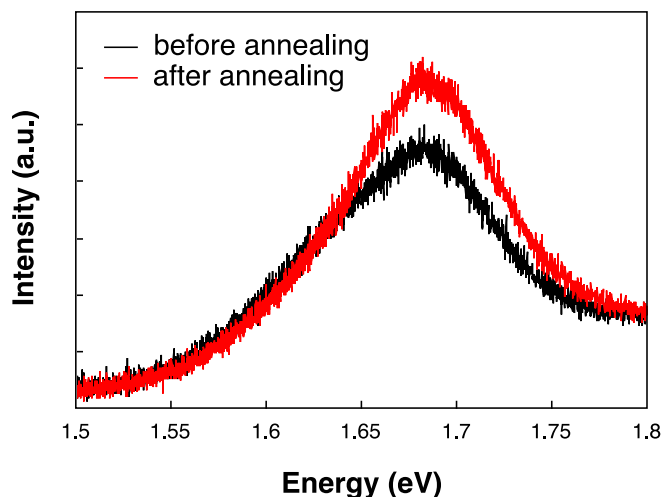

Figure S10. Photoluminescence of transferred Janus SMoSe monolayer on SiO_2/Si substrate before and after annealing at 305 ^{o}C for 2h.
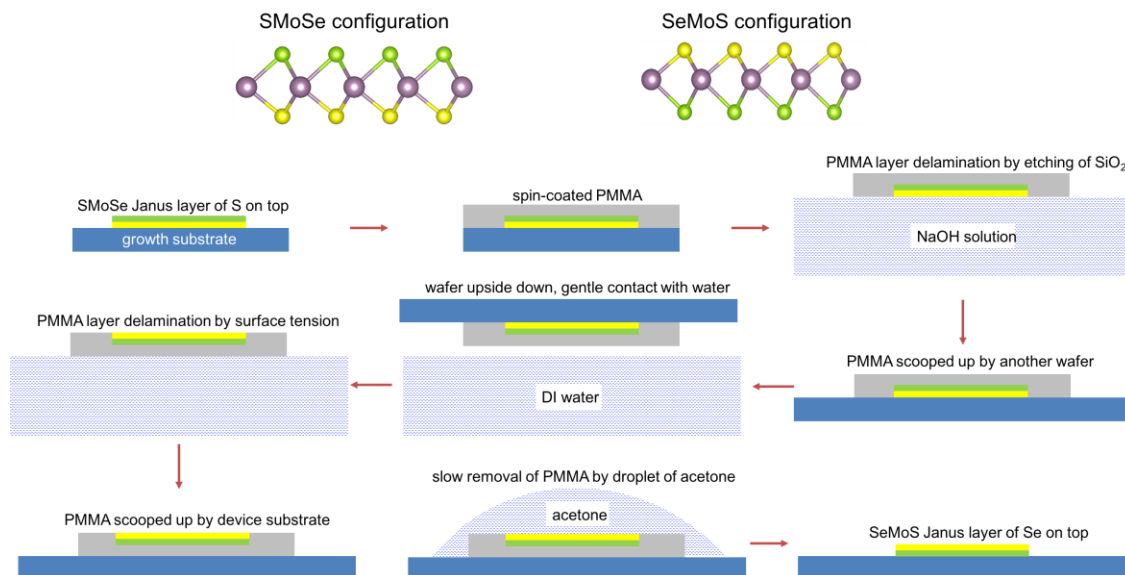
Figure S11. Schematic illustration of the SeMoS Janus structure (Se layer on top, S layer at bottom) preparation on the device substrate starting from the SMoSe Janus structure (S layer on top, Se layer at bottom).

Table S1. Summary of the experimental and computational results regarding on the A_{1g} and E^1_{2g} vibrations modes of the monolayer MoSe$_2$, Janus SMoSe and MoS$_2$.

	Experiment (cm^{-1})		Computation (cm^{-1})	
	A_{1g}	E^1_{2g}	A_{1g}	E^1_{2g}
MoSe$_2$	240	287	234.9	276.9
SMoSe	290	350.8	283.1	341.5
MoS$_2$	404	383	396.3	373.1

1. Voiry, D.; Yamaguchi, H.; Li, J. W.; Silva, R.; Alves, D. C. B.; Fujita, T.; Chen, M. W.; Asefa, T.; Shenoy, V. B.; Eda, G.; Chhowalla, M. Enhanced Catalytic Activity in Strained Chemically Exfoliated WS$_2$ Nanosheets for Hydrogen Evolution. *Nat. Mater.* **2013**, *12*, 850-855.
2. Chase Jr, M. Tables, Nist-Janaf Thermochemical. *J. Phys. Chem. Ref. Data, Monograph* **1998**, *9*, 1-1951.
3. Najmaei, S.; Liu, Z.; Zhou, W.; Zou, X.; Shi, G.; Lei, S.; Yakobson, B. I.; Idrobo, J.-C.; Ajayan, P. M.; Lou, J. Vapour Phase Growth and Grain Boundary Structure of Molybdenum Disulphide Atomic Layers. *Nat. Mater.* **2013**, *12*, 754-759.
4. Tonndorf, P.; Schmidt, R.; Bottger, P.; Zhang, X.; Borner, J.; Liebig, A.; Albrecht, M.; Kloc, C.; Gordan, O.; Zahn, D. R. T.; de Vasconcellos, S. M.; Bratschitsch, R. Photoluminescence Emission and Raman Response of Monolayer MoS$_2$, MoSe$_2$, and WSe$_2$. *Opt. Express* **2013**, *21*, 4908-4916.

5. Lu, X.; Utama, M.; Lin, J.; Luo, X.; Zhao, Y.; Zhang, J.; Pantelides, S. T.; Zhou, W.; Quek, S. Y.; Xiong, Q. Rapid and Nondestructive Identification of Polytypism and Stacking Sequences in Few-Layer Molybdenum Diselenide by Raman Spectroscopy. *Adv. Mater.* **2015**, *27*, 4502-4508.

6. Nam, D.; Lee, J. U.; Cheong, H. Excitation Energy Dependent Raman Spectrum of $MoSe_2$. *Sci. Rep.* **2015**, *5*.